KeA1

CHINESE ROOTS
GLOBAL IMPACT

Contents lists available at ScienceDirect

Green Chemical Engineering

journal homepage: www.keaipublishing.com/en/journals/green-chemical-engineering



Article

Environmentally sustainable production of biodiesel from low-cost lipid feedstock using a zirconium-based metal-organic framework sulfonated solid catalyst



Balkis Hazmi a , Umer Rashid a,b,* , Bryan R. Moser c , Mohd Hafizuddin Ab Ghani a , Fahad A. Alharthi d , Jeehoon Han e,* , Jiyun Yoo e

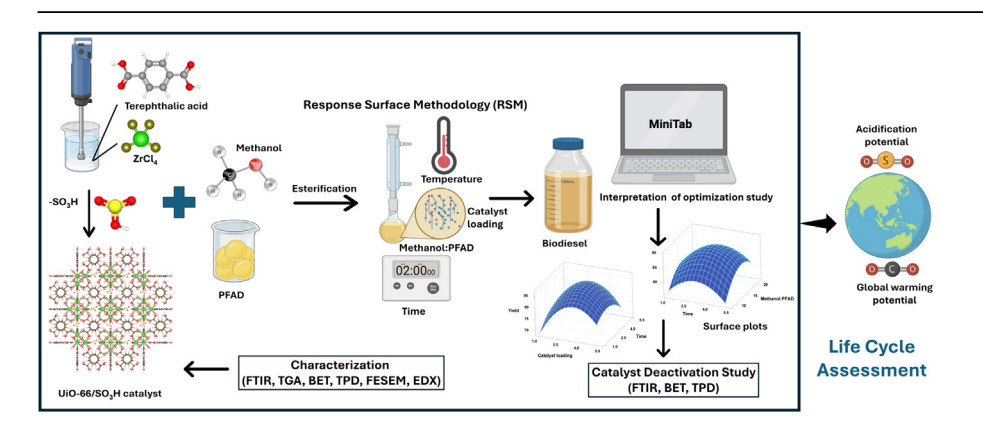
- ^a Institute of Nanoscience and Nanotechnology, Universiti Putra Malaysia (UPM), 43400, UPM, Serdang, Selangor, Malaysia
- b Center of Excellence in Catalysis for Bioenergy and Renewable Chemicals (CBRC), Faculty of Science, Chulalongkorn University, Bangkok, 10330, Thailand
- ^c United States Department of Agriculture, Agricultural Research Service, National Center for Agricultural Utilization Research, Bio-Oils Research Unit, Peoria, IL, 61604, USA
- ^d Chemistry Department, College of Science, King Saud University, Riyadh, 1145, Saudi Arabia
- e Department of Chemical Engineering, Pohang University of Science and Technology (POSTECH), Pohang, Gyeongbuk, 37673, South Korea

HIGHLIGHTS

UiO-66/SO₃H is highly active for catalytic esterification of PFAD to biodiesel.

- Catalytic optimization was performed utilizing central composite design.
- The UiO-66/SO₃H catalyst was reusable and stable for up to 7 consecutive
- Life cycle analysis revealed that the acidification potential of PFAD biodiesel was low.

GRAPHICAL ABSTRACT



ARTICLE INFO

Keywords: Fatty acid methyl esters Metal-organic framework Palm fatty acid distillate Response surface methodology Life-cycle assessment

ABSTRACT

Heterogeneous acidic Zr-MOF (metal-organic framework) catalyst, UiO-66/SO $_3$ H was synthesized for palm fatty acid distillate (PFAD)-methanol esterification. The characterizations for catalyst precursor and active catalyst were carried out using infrared spectroscopy, ammonia-temperature desorption analysis, thermogravimetric analyser, X-ray diffraction, surface textural analyser, and field emission scanning microscopy. The surface area of UiO-66 and UiO-66/SO $_3$ H was 714.77 m 2 /g and 503.02 m 2 /g, respectively. Meanwhile, the acidity strength shown an increase in values, rising from 3.14 mmol/g to 7.98 mmol/g. Throughout the catalytic screening test under fixed parameters, UiO-66/SO $_3$ H produced 72.3% of fatty acid methyl ester (FAME) while 45.9% catalyzed by UiO-66. Then, UiO-66/SO $_3$ H was selected for response surface methodology-central composite design (RSM-CCD) optimization. Following 31 experiments, the optimized conditions were determined to be 75 °C, 1.3 h, 4.2 wt% catalyst, and a methanol to PFAD molar ratio of 21:1, resulting in a yield of 98.6% FAME. Reusability

E-mail addresses: umer.rashid@upm.edu.my (U. Rashid), jhhan@postech.ac.kr (J. Han).

https://doi.org/10.1016/j.gce.2024.10.001

^{*} Corresponding authors.

tests demonstrated that the catalyst maintained its activity for seven cycles, averaging 72.4% yield but subsequently dropping to 53.8% after the eighth cycle. Environmental sustainability was evaluated using life-cycle assessment (LCA) across seven impact categories: global warming potential, stratospheric ozone depletion, acidification potential, terrestrial ecotoxicity, freshwater ecotoxicity, marine ecotoxicity, and fossil resource scarcity. LCA analysis revealed that the PFAD process had a substantial global warming impact, with the exception of microalgae-based biodiesel. The PFAD process has lower acidification potential than soybean or lignocellulosic biomass. Our advanced biodiesel production method, with minimal methanol and low electricity, is an environmentally friendly alternative.

1. Introduction

One such renewable energy source that has gained attention owing to its biodegradability and sustainability is biodiesel, which is defined as an alternative diesel fuel composed of mono-alkyl esters of long-chain fatty acids derived from lipids [1]. Biodiesel is miscible in any proportion with diesel fuel and generally possesses a superior cetane number, resulting in faster autoignition and lower nitrogen oxide formation during combustion in compression-ignition (diesel) engines [2]. The simplest method for biodiesel production is (trans)esterification of vegetable oils, animal fats, or other lipids with a stoichiometric excess of a short-chain alcohol (methanol or ethanol) in the presence of a homogeneous catalyst. These common liquid phase-catalysts, such as H₂SO₄, HCl, H₃PO₄, ClSO₃H, KOH, NaOH, KOCH₃, and NaOCH₃ are known in facilitating rapid reaction rate due to homogeneity with reaction mixture [3,4]. However, the main challenges in utilization of homogeneous catalysts include non-reusability, the discharge of substantial quantities of effluent during purification, and the potential corrosion to industrial reactors, which results in increased operational costs [5].

Alternatively, heterogeneous catalysts have been developed that mitigate these deficiencies. Heterogeneous catalysts can be acidic, basic, or both and are bound to any of several solid supports with high surface area, such as metal oxides, activated carbon, alumina, ionic liquid, and silica [6]. For instance, Huang et al. [7] prepared photothermal super basic potassium mono-atom embedded on graphene sheet (K-SAG) catalysts that successfully processed *Xanthium sibiricum* oil into biodiesel (99.6%) at room temperature. A microporous 2,5-furandicarboxylic (FDCA)/SA-Hf metal-organic framework (MOF) catalyst (1080 m²/g, 1.89 nm) derived from biomass lignocellulosic ligand, 2,5-furandicarboxylic (FDCA) acid, coordinated with hafnium chloride (HCl₄), and followed by stearic acid (SA) functionalization. The catalyst achieved a 98.6% conversion to methyl oleate and maintained a yield of over 90% across six reuse cycles, attributed to its high wettability and hydrophobicity characteristics [8].

MOFs have attracted considerable attention in recent time owing to their diverse range of applications, including catalysis, CO₂ capture, drug delivery, water waste treatment and adsorption of heavy metals and dyes [9,10]. MOFs are highly favored as catalyst precursors because of their unique surface properties, such as high surface area, porosity, and pore size flexibility, which enable the even distribution of active components within the framework [11,12]. For example, sulfonic acid functionalization of MIL-100(Fe) produced a catalyst that successfully esterified oleic acid to methyl oleate in 95.86% yield after 2 h and was reusable for up to seven reaction cycles [13]. A Co-N_x bifunctional catalyst derived from pyrolyzed ZiF-67 with enhanced acidity and basicity successfully catalyzed transesterification of microalgal lipids at an optimized yield of 96.7% [14]. In another example, a Mo-MOF with a rod-like monoclinic crystal structure was synthesized from Na₂MoO₄ and 4-piperidinecarboxvlic acid and was used to convert oleic and palmitic acids to the corresponding methyl esters in nearly 100% yield [15].

Studies found that zirconium-based MOF known as UiO-66 are thermally stable up to 500 °C and possesses a water-tolerant structure which is mechanically and chemically stable over a broad pH range [16]. These remarkable features make UiO-66 an excellent option as a catalyst supportive material. Nowadays, the utilization of heteropoly

acids immobilized on MOF structure for active site functionalization has gained attention due to their low corrosivity and high Brønsted acidity [17]. For example, immobilization of 12-tungstophosphoric acid (HPW) on UiO-66 was shown by Ma et al. [18] for *n*-butyl acetate production. Upon immobilization, the crystallinity patterns were unchanged, indicating no impurities and the optimized 30HPW@UiO-66 catalyst achieved 80% yield of *n*-butyl acetate under the stated conditions of 120 °C, 2:1, 3 wt% and 3 h. Next, a UiO-66/SFN catalyst derived from ammonium sulfate impregnated on UiO-66 followed by N2 carbonization at 500 °C was utilized in oleic acid-methanol esterification. The reaction required 8 wt% of UiO-66/SFN, 8:1 of methanol-oleic acid molar ratio, 70 °C heating temperature and 2 h of reaction time to achieve 96.2% of methyl oleate [18]. Nevertheless, studies on MOF-supported catalysis for the esterification of biodiesel derived from long-chain polyunsaturated fatty acids (LC-PUFAs), such as waste cooking oil, palm fatty acid distillate, and animal fats, are still limited. Yusuf et al. [19] reported an adequate active surface area (827 m²/g) and acidity (0.196 mmol/g) of 7% CuO/UiO-66 catalyst that esterified waste cooking oil (WCO) to biodiesel with a yield of 90.1% within 4 h and 160 °C. Microwave-assisted catalytic transesterification of soybean oil catalyzed by an alkali UiO-66 composite catalyst, CaO-ZrO2 (3.9 mmol/g), achieved a yield of 98.03% with a high catalyst loading of 6.5 wt% and was heated at a temperature beyond the methanol boiling point at 73.1 °C within 1.1 h of reaction time to utilize a lower methanol-to-oil ratio of 9.7:1 [20]. Additional studies of UiO-66 active site modification are still necessary to guarantee the suitability of catalyst-feedstock characteristics for optimal fatty acid methyl ester (FAME) generation.

Response surface methodology (RSM) is a derived formula combination between mathematical and statistical that useful in improving and optimizing the biodiesel production's process variables [21]. RSM can reduce the number of experiments by merging two variables or more simultaneously in the response of biodiesel yield as comparison to conventional method that opted single variable [22]. The significance level for the individual variable, variables interaction and optimization can be determined as the indication is known when the p-value <0.05. For instance, a study found that the p-value of these parameters and interactions of second-order model, A², B², C², A, B, C, and AC (A: methanol-oil ratio, B: temperature, C: catalyst loading) were meaningful for esterification of *Quercus brantii Lindl* oil [23]. Besides, *p*-value <0.05, the order of independent reaction factors significancy also can be accessed via F-value as per revealed in analysis of variance (ANOVA) table [24]. Research by Zheng et al. [25] adopted full quadratic function for transesterification of Koelreuteria integrifoliola oil catalyzed by mesoporous bifunctional acid-base MP-ZnF, emphasizing that time is the most significant factor of the reaction due to its highest F-value score (1348).

Life-cycle assessment (LCA) is a vital tool that systematically gathers data on inputs and outputs to quantify the environmental footprint associated with biodiesel production [26]. This comprehensive assessment examines various factors, such as inputs, processes, infrastructure, and equipment, among others [26]. In the context of catalyst utilization within biodiesel production, there arises a compelling need for environmental assessments to scrutinize and predict the potential long-term ecological impacts [27]. When evaluating the environmental impact of biodiesel production using waste palm (cooking) oil and a heterogeneous

catalyst composed of calcium oxide derived from chicken eggshells, it is important to consider the differences in $\rm CO_2$ emissions when compared to the homogenous potassium hydroxide method. This distinction can significantly affect the contribution to climate change, as demonstrated in a study by Mu et al. [28]. For example, optimization esterification microalgae biodiesel (96.8%) by acidic graphene like catalyst (S-NGL-600) conducted by Huang et al. [29] in a light induced photothermal assembly showed better performance compared to conventional $\rm H_2SO_4$ catalyst as the LCA predicting the 0.87 MJ/MJ energy-saving and $\rm -89.42~CO_2eq/MJ$ environment protection, respectively. This study explores the critical role of LCA in evaluating the sustainability of biodiesel and delves into the intricate dynamics of environmental considerations, shedding light on the environmental implications of catalysts in biodiesel production.

This implies that the UiO-66/SO₃H catalyst has not yet been utilized to demonstrate its effectiveness in the esterification of palm fatty acid distillate using palm fatty acid distillate (PFAD) as the feedstock. In this study, we aimed to produce UiO-66/SO₃H by functionalizing UiO-66 with sulfonate groups, and subsequently tested this acidic catalyst for the esterification of waste PFAD, a low-cost residue obtained from the palm oil refining process. To examine the physical and chemical properties of the pristine and post-functionalized samples, we conducted thermogravimetric analysis (TGA), ammonia-thermal desorption analysis (NH3-TPD), infrared spectroscopy, Brunauer-Emmett-Teller (BET) surface area analysis, and field-emission scanning electron microscopy equipped with energy dispersive X-ray spectroscopy (FESEM-EDX). Additionally, we used a response surface methodology-central composite design (RSM-CCD) to optimize the production of biodiesel from PFAD and evaluated the impact of reaction variables on biodiesel yield. We also conducted catalyst reusability experiments and compared the properties of the spent catalysts with those of a fresh UiO-66/SO₃H catalyst. Furthermore, this study aimed to systematically analyze the environmental footprint of biodiesel production and establish a sustainable production pathway from biowastes, specifically palm oil, with a specific focus on the catalytic role of UiO-66/SO₃H.

2. Experimental section

2.1. Materials

All solvents and chemicals, including methanol (99.8%, R&M), n-hexane (99.8%, R&M), dimethylformamide (99.5%, R&M), zirconium oxychloride octahydrate (ZrOCl $_4$ ·8 H_2 O, AR grade, QRëC), benzene-1,4-dicarboxylic acid (BDC, 98.0%, Sigma-Aldrich), sulfuric acid (H_2 SO $_4$, 98.0%, R&M), acetic acid (C H_3 COOH, 98%, R&M), and hydrochloric acid (HCl, 37%, R&M), were analytical reagent grade and used without further purification. PFAD was obtained from a local palm oil refinery in Malaysia.

2.2. Preparation of UiO-66 and UiO-66/SO $_3H$

ZrOCl $_4$ ·8H $_2$ O (5 mmol) and BDC (7.5 mmol) were dispersed in a mixture of dimethylformamide (30 mL) and acetic acid (2 mL), followed by the addition of HCl (1.5 mL) dropwise. The mixture was transferred to a Teflon-lined reactor for crystallization at pressurized conditions at 160 °C for 12 h. After cooling to room temperature, the suspension was transferred to a centrifuge tube and separated from DMF. The UiO-66 sample was washed with methanol and ethanol to remove unreacted linker. The washed UiO-66 suspension was dried overnight in a vacuum oven at 120 °C to obtain UiO-66 as an activated powder. Activated UiO-66/SO $_3$ H was sulfonated by soaking in 50 mL of 1 M H $_2$ SO $_4$ and refluxing for 30 min at 150 °C. After the sample was subjected to sulfonation, it was washed with warm distilled water to remove any excess H $_2$ SO $_4$. The sample was then left to dry overnight at a temperature of 100 °C in an oven.

2.3. Catalyst characterization

The Agilent Cary 630 attenuated total reflectance Fourier transform infrared spectrometer was utilized to identify the functional groups and bonding interactions of MOF and sulfonated MOF. The analysis was conducted within the range of 4000 to 650 cm⁻¹ using 32 scans and a spectral resolution of 8 cm⁻¹. Surface area and porosity of a degassed UiO-66 sample were measured using nitrogen adsorption-desorption isotherms at $-196.15\ ^{\circ}\text{C}$ with a Micrometrics Tristar II Plus surface analyzer. Microscopic morphology of platinum precoated UiO-66 and UiO-66/SO₃ samples were observed using an FEI Novananosem 230 FESEM at 200 K magnification power. Elemental compositions were determined by an Oxford instrument Max 20 energy dispersive x-ray spectrometer (EDX). TGA was performed using a Mettler Toledo TGA under inert nitrogen flow from 25 to 600 °C with a temperature ramp rate of 10 °C/min. Acidity was measured using NH3-TPD, which was equipped with a thermal conductivity detector (TCD). The chemisorption process was carried out by absorbing NH3 in helium gas at a flow rate of 30 mL/min, while simultaneously heating the system from 50 to 950 °C during absorption and desorption.

2.4. Esterification

A single batch reactor equipped with a condenser and thermocouple was utilized for catalytic esterification of PFAD. A fixed weight of PFAD (approx. 10 g) was mixed and continuously stirred with known amounts of catalyst (1 wt% – 5 wt%) and methanol (methanol:PFAD molar ratios of 9:1–21:1) and heated (75–125 °C) for 1–5 h. Excess methanol was removed from the esterified PFAD using a rotary evaporator. The UiO-66/SO₃H catalyst was then separated from biodiesel using gravitational filtration. Lastly, the biodiesel was washed with hot distilled water and dried with ammonium sulfate.

2.5. Design of experiment and statistical analysis

The experimental design for optimizing PFAD esterification was selected as RSM-CCD. The design comprised five levels of four factors, including catalyst loading (wt%), methanol-to-PFAD molar ratio, reaction time (h), and temperature (°C), resulting in 31 experimental runs in a randomized order, as presented in Table 1. The statistical analysis was performed by Minitab ν 21 statistical software. The significant factors and their interactions were calculated by ANOVA, where the significant level was set at 95% with a p-value of 0.05. A correlation coefficient (R²) was obtained through a model fitting equation correlating the interaction between the response variable and independent variables, as given in Eq. (1).

$$\text{Yield }(\%) = \gamma_0 + \sum_{i=1}^k \gamma_i X_i + \sum_{i=1}^k \gamma_{ii} X_i^2 + \sum_{i < j}^k \gamma_{ij} X_i X_j + \varepsilon \tag{1}$$

where Yield (%) is the response, γ_0 is the intercept, γ_i is the linear coefficient, γ_{ii} is the interaction coefficient, γ_{ij} is the quadratic coefficient, and X_i and X_i are independent variables.

Table 1
Factors and levels investigated during RSM-CCD optimization of PFAD esterification using UiO-66/SO₃H catalyst.

Factor	Code	Level				
		-2	-1	0	1	2
Catalyst loading (wt%)	A	1	2	3	4	5
Time (h)	В	1	2	3	4	5
Methanol-to-PFAD molar ratio	С	9	12	15	18	21
Temperature (°C)	D	75.0	87.5	100.0	112.5	125.0

2.6. Catalyst reusability

Catalyst reusability was evaluated by mixing 4.2 wt% of recovered UiO-66/SO $_3$ H catalyst with methanol (methanol:PFAD molar ratio of 21:1). PFAD was esterified at constant optimized conditions of 1.3 h and 75 °C. At the end of each reaction cycle, biodiesel and spent catalyst were separated by gravity filtration. The catalyst was then washed with n-hexane and dried overnight at 105 °C. The catalytic esterification cycles were repeated for 8 cycles and yields were determined by gas chromatography (GC) following EN 14103.

2.7. Biodiesel yield analysis

An Agilent 7890A GC equipped with a flame ionization detector (FID) and a polar capillary column (BPX-70, 60 mm \times 0.25 mm \times 0.25 mm) was used for determination of biodiesel yield following EN 14103. The biodiesel sample was combined with a 1000 ppm solution of methyl heptadecanoate in n-hexane to produce a diluted solution. One microliter of the diluted biodiesel was then injected into the system at a temperature of 250 °C. At this temperature, the fatty acid methyl ester (FAME) components of biodiesel were vaporized and carried by hydrogen gas. The oven temperature gradually increased from 100 to 250 °C at a rate of 10 °C per minute. The eluted FAME components were identified by comparing their retention times of reference FAMEs in elution order of methyl myristate, methyl palmitate, internal standard (IS), methyl stearate, methyl oleate, and methyl linoleate, respectively. Percent biodiesel yield was determined following Eq. (2).

Yield (%) =
$$\frac{\sum (A_{ME} - A_{IS})}{A_{IS}} \times \frac{C_{IS} \times V_{IS}}{Wt} \times 100$$
 (2)

where A_{ME} is the area of methyl ester, A_{IS} is the area of the internal standard, C_{IS} is the concentration of the internal standard, W_t is the weight of biodiesel, and V_{IS} is the volume of the internal standard.

2.8. Life-cycle assessment (LCA) of biodiesel production

Utilizing established LCA methodologies, as outlined by ISO 14040 and 14044 standards, four key phases were incorporated: goal and scope definition, life cycle inventory analysis, impact analysis, and interpretation [30]. Employing this methodology, a LCA was implemented to evaluate the environmental implications of biodiesel production from PFAD using the UiO-66/SO₃H catalyst. The LCAs were performed using SimaPro commercial software, drawing upon the comprehensive Ecoinvent database [31]. To maintain precision, the system boundary was carefully defined, encompassing the cradle-to-gate commencing with PFAD and culminating in biodiesel (as depicted in Fig. 1), while exempting impacts arising from the UiO-66/SO₃H catalyst preparation. The functional unit for analysis was set at 1 kg of biodiesel, and evaluations were conducted across seven key environmental impact categories: global warming potential (GWP), stratospheric ozone depletion (SOD), acidification potential (ACP), terrestrial ecotoxicity (TETP), freshwater ecotoxicity (FETP), marine ecotoxicity (METP), and fossil resource scarcity (FRS).

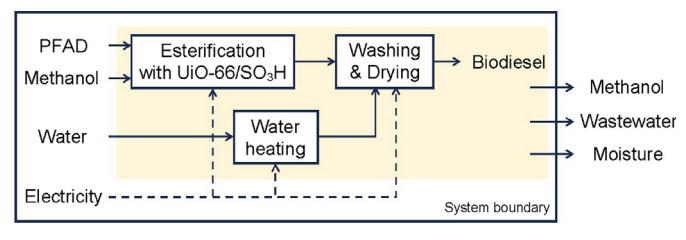


Fig. 1. Block flow diagram of biodiesel production using UiO-66/SO₃H catalyst.

In the biodiesel production process, a combination of resources was utilized, including PFAD, the UiO-66/SO $_3$ H catalyst, water, methanol, and electricity, as detailed in Table 2. Typically, PFAD emerges as a consequential waste product of the palm oil refining process, which primarily aims to yield refined palm oil (RPO) [32]. In the realm of LCA frameworks, PFAD is variously regarded as a residue, byproduct, or coproduct, with each classification carrying distinct environmental impact allocations. To comprehensively address variability, this study undertakes LCA in alignment with all three classifications, building upon prior work by Xu et al. [32].

3. Results and discussion

3.1. Fourier transform infrared spectroscopy (FTIR) analysis of UiO-66 and UiO-66/SO₃H catalysts

The FTIR spectra of UiO-66 and UiO-66/SO $_3$ H are depicted in Fig. 2a. The broad absorption bands at 3500-3200 cm $^{-1}$ were due to the stretching bands of OH from adsorbed moisture and residual solvent (DMF). Absorption bands associated with symmetrical C=O, asymmetrical O-C=O, and C-O stretching vibrations of the MOF were detected at 1675, 1413, and 1018 cm $^{-1}$, respectively [33,34]. The bands at 1569 cm $^{-1}$ and 1514 cm $^{-1}$ were attributed to stretching absorption of the C=C bonds of benzene rings [33] from the organic ligand and terephthalic acid. A symmetric vibration absorption band at 726 cm $^{-1}$ was correlated with the coordination of Zr $^{4+}$ with terephthalic acid by formation of O-Zr–O bonds [20]. Two additional absorption bands at 1055 and 674 cm $^{-1}$ on UiO-66/SO $_3$ H confirmed the presence of the sulfonate and hydroxy groups [16,20], thereby indicating that sulfonation of UiO-66 was successful.

3.2. Thermal degradation analysis of UiO-66 and UiO-66/SO₃H catalysts

Fig. 2b depicts the thermal degradation curves of UiO-66 and UiO-66/SO $_3$ H, as determined by TGA under an inert (N $_2$) atmosphere. The first degradation stage of both samples (21–210 °C) was due to removal of moisture and adsorbed solvent [35] from the surfaces of UiO-66 and UiO-66/SO $_3$ H, with weight losses of 1.36 wt% and 12.82 wt%, respectively. The weight loss of 14.87 wt% occurring at 210–345 °C was attributed to the decomposition of the sulfonate groups and complete removal of solvent molecules from UiO-66/SO $_3$ H [36–38]. Dihydroxylation of zirconium oxo-clusters and organic linkers of UiO-66 and sulfonated UiO-66 were recorded at 345–480 °C by mass losses of 90.06 wt% and 6.45 wt%, respectively, indicating that thermal stability was significantly improved after sulfonate functionalization [39]. Further degradation at temperatures above 480 °C was attributed to the residual phase of UiO-66 [40].

3.3. BET surface properties of UiO-66 and UiO-66/SO₃H catalysts

MOF surface properties were measured by the N_2 absorption technique, as shown in Fig. 2c and Table 3. The UiO-66 and UiO-66/SO₃H

Table 2Inventory data for production of biodiesel using UiO-66/SO₃H catalyst based on the functional unit (1 kg of biodiesel).

Input			Output		
Flow	Value	Unit	Flow	Value	Unit
UiO-66/SO ₃ H catalyst	0.0424	kg	Biodiesel	1	kg
UiO-66 support	0.5053	kg	UiO-66/SO ₃ H catalyst	0.0444	kg
Water	10.1061	kg	Wastewater	10.1061	kg
Methanol	2.8934	kg	Methanol	2.3295	kg
PFAD	1.0106	kg	Moisture	0.0005	kg
Electricity	6.1	kWh			

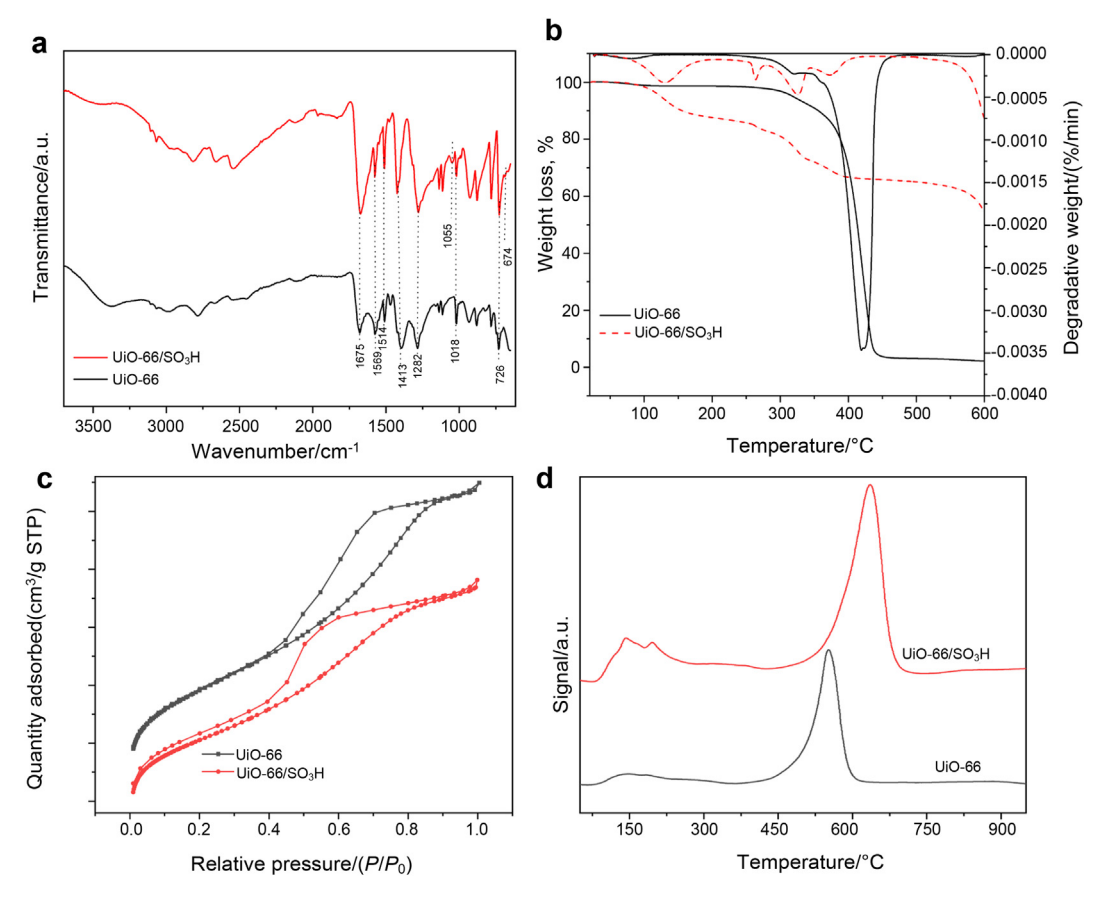


Fig. 2. UiO-66 and UiO-66/SO₃H analysis using (a) FTIR spectroscopy, (b) material stability degradation test, (c) textural surface measurement, and (d) temperature programmed acidity strength measurement.

Table 3 Surface property analysis of UiO-66 and UiO-66/SO $_3$ H using the N $_2$ adsorption-desorption technique.

Catalyst	Surface area/(m ² /g)	Pore volume/ (cm ³ /g)	Average pore size/nm	Total NH ₃ absorption/ (mmol/g)
UiO-66	714.77	0.56	4.26	3.14
UiO-66/ SO ₃ H	503.02	0.25	3.30	7.98

materials demonstrated hysteresis loops with type-IV isotherms indicative of a bimodal micro-mesoporous framework. These micromesoporous structures were categorized as H2, implying narrow and disordered pores of MOF interconnected with metal centers and organic ligands, which was also observed previously in pore width distribution plots [41,42]. The surface area of UiO-66 was measured at 714.77 m²/g, while the post-sulfonated material had a surface area of 503.02 m²/g. The decrease in surface area after sulfonation indicated that the sulfonate ions were impregnated and packed onto the surface and inside cavities of the UiO-66 mesoporous structure [12]. This was confirmed by average pore size measurements of 4.26 and 3.30 nm for UiO-66 and UiO-66/-SO₃H, respectively, as determined by the Barrett, Joyne, and Halenda (BJH) method. The reduction of pore volume from 0.56 to 0.25 cm³/g after sulfonation confirmed pore blockage and pore depth reduction due to the dispersion of sulfonate groups onto the surface of UiO-66 which agrees with Tang et al.'s findings [43]. We speculate that the resulting pore size and volume reduction produced specific active sites for catalytic esterification that facilitated effective diffusion of fatty acids and methanol molecules in the formation of FAME [44]. Furthermore, it appears that an improperly sized catalyst pore that is larger than the molecules of the reactants is effortlessly deactivated, perhaps as a result of an uncontrollably high diffusion rate that amplifies active site masking or leaching during the esterification reaction [45].

3.4. Catalyst acidity of UiO-66 and UiO-66/SO₃H catalysts

The acidity properties of UiO-66 and UiO-66/SO₃H were probed by NH₃-TPD, as shown in Fig. 2d and Table 3. Intense peaks of ammonia absorption-desorption formed at 400-700 °C, which were attributed to strong Brønsted acidity [46] for both UiO-66 and UiO-66/SO₃H. As expected, the total acidity of UiO-66/SO₃H (7.98 mmol/g) was higher than for UiO-66 (3.14 mmol/g). The desorption pattern of UiO-66/SO₃H occurred at a higher temperature and intensity than UiO-66, which was attributed to the encapsulation of SO₃H groups inside the framework. Lastly, the weak desorption peak at 143 °C in UiO-66/SO₃H was attributed to the desorption of ammonia from sites of weak acidic strength, which contributed overall acidic strength to the catalyst [47]. These results suggested that the UiO-66/SO₃H catalyst had excellent overall acidic strength toward catalytic esterification of PFAD into FAME primarily due to its high acid density which drives the reaction forward. The presence of sulfonate group (- SO_3H) increases the acid strength by offering additional protonic active sites (H⁺) to enable fatty acid carbon protonation on active pores, followed by methanol's nucleophilic attack to form an ester bond [48] where UiO-66/SO₃H demonstrated more yield than UiO-66 in the esterification screening test.

3.5. Catalyst morphology of UiO-66 and UiO-66/SO₃H catalysts

Fig. 3 shows the microstructure of Zr-based metal organic frameworks magnified at 50 k. The UiO-66 material (Fig. 3a) exhibited near-cubic

particles of relatively consistent size. However, in Fig. 3b, UiO-66/SO $_3$ H displayed an irregular agglomerated pattern of blocky-shaped particles due to the electrostatic interaction between sulfonate ions and the parent framework structure. The elemental analyses of UiO-66 and UiO-66/SO $_3$ H are reported in Table 4. As anticipated, both samples contained C, O, and Zr. However, S was detected exclusively in the UiO-66/SO $_3$ H sample after sulfonation. The incorporation of a sulfonate group resulted in a slightly higher oxygen weight percentage in UiO-66/SO $_3$ H. Additionally noteworthy was the lower relative amounts of C and Zr in UiO-66/SO $_3$ H, which was once again attributed to sulfonation.

3.6. Catalyst screening and optimization via RSM-CCD model analysis

The methanolysis of PFAD catalyzed by UiO-66 and UiO-66/SO₃H was investigated and compared under fixed reaction parameters at 2 wt %, 9:1 of methanol-PFAD ratio and reaction temperature at 75 °C with reaction time ranging from 1 to 5 h, as depicted in Fig. 4a. The curves showed that FAME yield increased with the extension of time (up to 4 h) of equilibrium reaction by maximizing the contact time for the methanol and fatty acids to reach active sites to convert into methyl ester [5,49]. The trends revealed that $UiO-66/SO_3H$ has better catalytic performance (51.7%-72.3%) compared to UiO-66 (32.5%-45.9%) due to synergic effect of sulfonate group, which provide high acidity to promote FAME conversion from high free fatty acid (FFA) feedstock [50]. Hence, the acidity from sulfonic group significantly contributed to the catalytic esterification. Additionally, the pore size distribution of both UiO-66 and UiO-66/SO₃H catalysts contributed to their catalytic performances. Abdullah et al. [44], mentioned that the palm-based fatty acid possessed 2.5 nm of approximate molecular diameter, therefore smaller average pore diameter of UiO-66/SO₃H (3.3 nm) was appropriate to enhance the diffusion of feedstocks to pack inside the acidic functionalized pores [51, 52] for the reaction to occur effectively than UiO-66 (4.26 nm). Further investigation of the reaction parameters and their interactions of PFAD catalyzed by UiO-66/SO₃H was studied using RSM-CCD approach.

The optimization of biodiesel synthesis from PFAD was conducted by RSM-CCD using 31 randomized experimental runs of 5 levels and 4 variable factors. The variables were catalyst loading (A), reaction time (B), methanol to oil molar ratio (C), and reaction temperature (D). A CCD design matrix with experimental and predicted yields was tabulated (Table 5). The experimental responses (biodiesel yields) were formulated through multiple regression analyses, such as linear, 2-way-interactions (2WI) and quadratic, to define an appropriate estimated coefficient RSM-model. The model that best fit biodiesel yield prediction was the second-order polynomial quadratic model depicted in Eq. (3) where the positive coefficient variables indicated positive effects on yield, while

Table 4 Elemental composition of UiO-66 and UiO-66/SO₃H.

Catalyst	Elemental composition, wt%					
	C O Zr S					
UiO-66	56.00	21.77	22.23			
UiO-66/SO ₃ H	52.28	28.25	14.47	4.00		

negative coefficient variables indicated the opposite.

$$\begin{aligned} \text{Yield (wt\%)} &= -18.4 + 10.24\text{A} + 8.86\text{B} + 7.461\text{C} + 0.970\text{D} - 2.352\text{A}^2 \\ &- 1.033\text{B}^2 - 0.1069\text{C}^2 - 0.004485\text{D}^2 - 0.409\text{AB} + 0.2060\text{AC} \\ &+ 0.0297\text{AD} + 0.0619\text{BC} - 0.0224\text{BD} - 0.04842\text{CD} \end{aligned} \tag{3}$$

The residual data set for 31 experimental runs also tabulated in Table 5, refer to the difference between the experimental biodiesel yield and predicted yield of the proposed regression model, which is a crucial measurement in consideration of model fitness. In Fig. S1a, the model for FAME yield was set to the normal probability plot in which the illustrated data points (percent yield against residual) were distributed in a linear pattern. The residual values were distributed randomly (refer to Fig. S1b) within the error range from -1 to 1 possessing the model fitness complementary for the actual results. In addition, the histogram residual plot (Fig. S1c) presenting the bell-shaped pattern confirmed the regression model equation accuracy and validity in Eq. (3). The residuals randomness fluctuation of observation orders around the center line behaving no correlation errors among the independent terms (Fig. S1d). Thus, analysis residual supports the model appropriately fit the experimental data.

The ANOVA test results and coefficient determination ($R^2 = 99.70\%$ and R^2 -adj = 99.44%) are summarized in Table 6. The RSM model estimation was considered reliable because the observed yields from experiments were close to the estimated yields. This result was also supported by a parity plot (Fig. 4b) of predicted yield versus experimental yield, with both side values distributed uniformly in a linear line. This demonstrated that the sets of data were in good agreement, revealing accurate estimation of biodiesel yield with respect to changes in the independent variables. Using a significance level of 5%, the model was found to be significant, with a p-value of < 0.0001 and a high F-value of 381.03. The adequacy of the model was also validated by non-significant lack of fit (p > 0.062), indicating that the theoretical model agreed closely with the experimental data.

Considering a 95% confidence interval, all interactions, except for the independent variable representing reaction time (B) as well as 2WI between reaction time and methanol to PFAD molar ratio (BC) and reaction

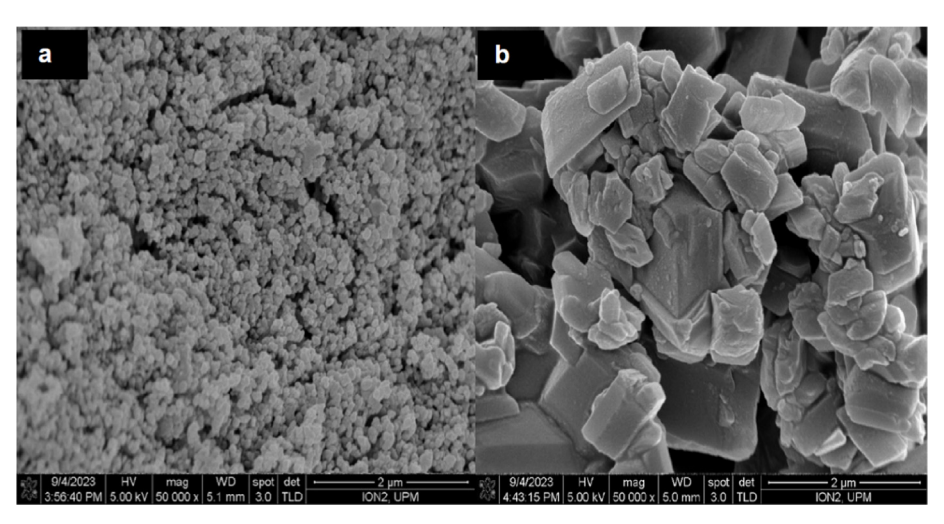


Fig. 3. FESEM images (50k magnification) of (a) UiO-66 and (b) UiO-66/SO₃H.

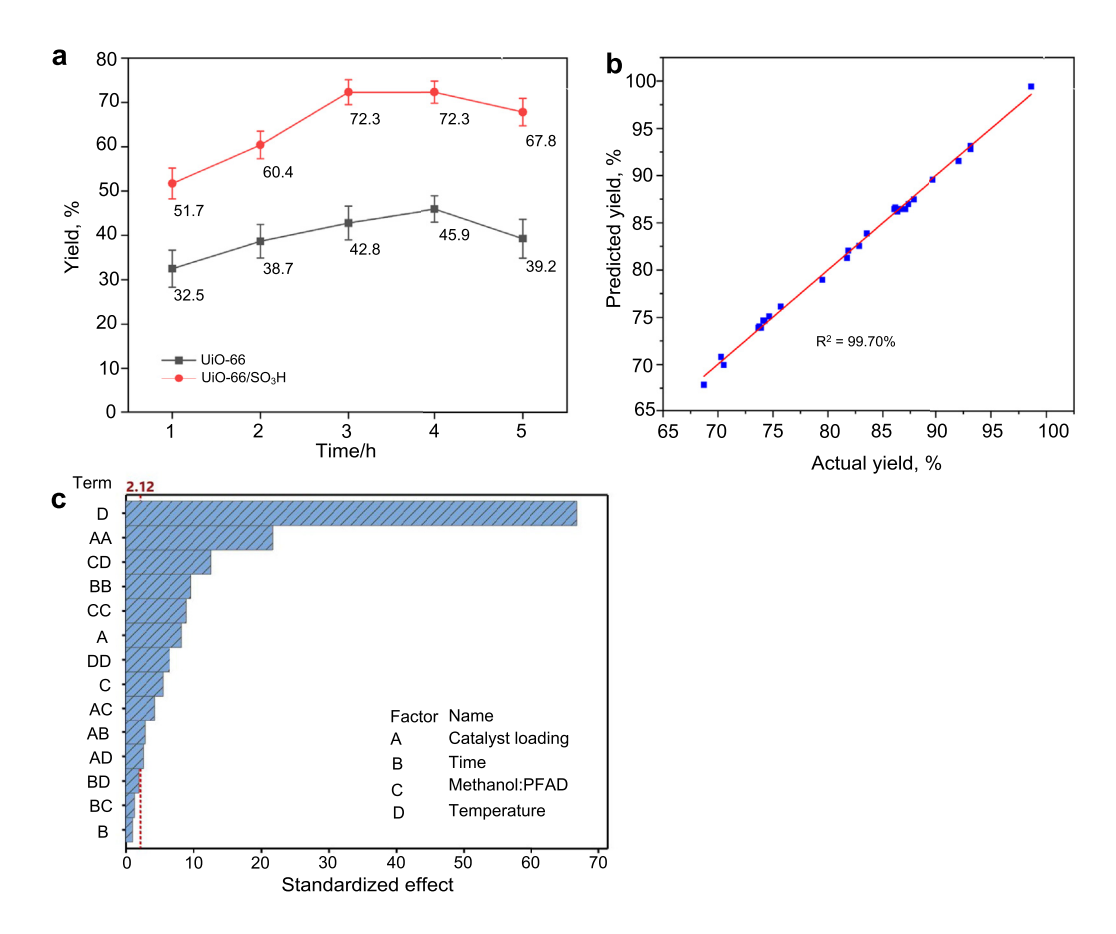


Fig. 4. (a) Catalyst screening at fixed temperature of 75 °C, 2 wt% catalyst loading and 9:1 methanol-PFAD ratio. (b) Parity plot of predicted biodiesel yield versus actual biodiesel yield. (c) Pareto chart of standardized variables ordered from most to least significant.

time and temperature (BD), were not significant (p > 0.05), as changes to these factors did not significantly affect biodiesel yield. The significance effect of the reaction variables and the interaction between the variables were arranged from the highest impact to the lowest impact by a Pareto chart, as seen in Fig. 4c. The sequence of the most to least significant reaction variables affecting biodiesel yield were as follows: D > AA > CD > BB > CC > A > DD > C > AC > AB > AD > BD > BC > B.

3.7. Influence of reaction parameters on biodiesel yield

The effect of changing various binary reaction parameters on biodiesel yield was carried out by RSM-CCD and interpreted in the form of a contour plot is shown in Fig. 5. The interaction of catalyst loading and reaction time on biodiesel yield is shown in Fig. 5a. Biodiesel yield increased proportionally to more than 85% when the catalyst load was increased from 1 to 3.8 wt% within reaction times of 1-4 h. As the number of catalytic active sites increased with longer reaction time, the methanol and fatty acid molecules were able to diffuse and remain on the active sites long enough for esterification to achieve maximum yield [53]. However, the yield decreased when esterification was performed with catalyst loads beyond 3.8 wt% and longer reaction time (> 4 h). Under such conditions, the reaction mixture became saturated, which led to mass transfer limitations between PFAD-methanol-catalyst, along with simultaneous hydrolysis up to 5 h, thus causing the reaction to digress towards reactants and lower biodiesel yield (< 75%) [54]. These results indicated that the highest yield can be achieved using moderate catalyst loadings and reaction times.

Fig. 5b illustrates the influence of catalyst loading and methanol to PFAD molar ratio at constant reaction temperature (100 $^{\circ}$ C) and time (3 h) on biodiesel yield. The yield increased from 70% to > 84% when

the catalyst loading was increased from 1 to 4 wt% at given methanol to PFAD molar ratio. The rate of reaction was improved proportionally with increases to methanol and catalyst levels until achieving an equilibrium state due to sufficient active sites for the methanol to infuse and react with PFAD [55–57]. Reversible effects promoting biodiesel yield reduction emerged when catalyst loadings approached 5 wt% due to the adsorption of FAME onto the available active sites of the catalyst, which hindered the absorption of unreacted fatty acids and thus reduced biodiesel yield [58]. This was similar to the findings of Maleki et al. [59] who reported that catalyst loads beyond the optimum amount enhanced unwanted mass transfer resistance.

The contour plots depicted in Fig. 5c-d and f represent the interaction of reaction temperature with catalyst loading, reaction time and methanol to PFAD molar ratio, respectively, on the yield of biodiesel from PFAD. As expected, the reaction rate increased with increasing temperature due to increased kinetic energy in the system. However, increases beyond an optimum temperature resulted in lower yields due to unwanted hydrolysis reactions and methanol vaporization [5,60]. As shown in Fig. 5c, at a fixed reaction time of 3 h and methanol to oil molar ratio of 15:1, yields of > 90% were obtained at reaction temperatures of 75-94 °C while yield decreased to 60% when the temperature was increased to 125 °C. As seen in Fig. 5d, yields of 90%-95% were achieved at reaction temperatures of 75-85 °C, but lower yields were observed when the reaction temperature was increased beyond 85 °C. The interaction of temperature and methanol to PFAD molar ratio on yield is displayed in Fig. 5f. The results indicated that yield approached 100% after 3 h at 75–80 °C with a catalyst loading of 3 wt%. On the contrary, catalyst loading, reaction time and methanol-PFAD molar ratio did not significantly affect yields, thereby proving that these variables were not correlated with yield, as predicted by the regression model.

Table 5Experimental and predicted yields for 31 esterification runs suggested by RSM-CCD.

Standard order	Run order	Catalyst loading, wt%	Time, h	Methanol:PFAD	Temperature, $^{\circ}\text{C}$	Yield,%	Predicted yield, wt%	Residue
6	1	4	2	18	87.5	93.15	92.783	0.367
24	2	3	3	15	125	68.72	67.858	0.862
20	3	3	5	15	100	82.85	82.540	0.310
7	4	2	4	18	87.5	92.07	91.521	0.549
28	5	3	3	15	100	86.02	86.439	-0.419
30	6	3	3	15	100	86.31	86.439	-0.129
23	7	3	3	15	75	98.64	99.413	-0.773
5	8	2	2	18	87.5	89.73	89.536	0.194
19	9	3	1	15	100	81.85	82.071	-0.221
29	10	3	3	15	100	86.51	86.439	0.071
10	11	4	2	12	112.5	75.71	76.150	-0.440
15	12	2	4	18	112.5	70.28	70.808	-0.528
22	13	3	3	21	100	83.53	83.886	-0.356
14	14	4	2	18	112.5	74.12	74.679	-0.559
26	15	3	3	15	100	87.04	86.439	0.601
8	16	4	4	18	87.5	93.15	93.131	0.019
13	17	2	2	18	112.5	70.52	69.945	0.575
3	18	2	4	12	87.5	87.82	87.459	0.361
21	19	3	3	9	100	81.74	81.295	0.445
31	20	3	3	15	100	86.05	86.439	-0.389
27	21	3	3	15	100	86.62	86.439	0.181
16	22	4	4	18	112.5	73.91	73.905	0.005
25	23	3	3	15	100	86.52	86.439	0.081
1	24	2	2	12	87.5	86.32	86.216	0.104
2	25	4	2	12	87.5	87.32	86.991	0.329
9	26	2	2	12	112.5	73.67	73.888	-0.218
4	27	4	4	12	87.5	86.13	86.596	-0.466
18	28	5	3	15	100	79.49	78.966	0.524
11	29	2	4	12	112.5	73.75	74.008	-0.258
12	30	4	4	12	112.5	74.24	74.632	-0.392
17	31	1	3	15	100	74.66	75.095	-0.435

Table 6ANOVA of the quadratic polynomial derived for prediction of biodiesel yield.

Source	DF	Adjusted sum of squares	Adjusted mean squares	F-Value	<i>p</i> - Value	Remark
Model	14	1782.79	127.34	381.03	0.000	Significant
Linear	4	1526.47	381.62	1141.86	0.000	Significant
A	1	22.48	22.48	67.28	0.000	Significant
В	1	0.33	0.33	0.98	0.336	Not
						Significant
C	1	10.08	10.08	30.15	0.000	Significant
D	1	1493.58	1493.58	4469.03	0.000	Significant
Square	4	190.76	47.69	142.70	0.000	Significant
AA	1	158.19	158.19	473.34	0.000	Significant
BB	1	30.53	30.53	91.35	0.000	Significant
CC	1	26.47	26.47	79.19	0.000	Significant
DD	1	14.04	14.04	42.02	0.000	Significant
2WI	6	65.56	10.93	32.70	0.000	Significant
AB	1	2.68	2.68	8.02	0.012	Significant
AC	1	6.11	6.11	18.29	0.001	Significant
AD	1	2.21	2.21	6.62	0.020	Significant
ВС	1	0.55	0.55	1.65	0.217	Not Significant
BD	1	1.26	1.26	3.77	0.070	Not Significant
CD	1	52.74	52.74	157.82	0.000	Significant
Error	16	5.35	0.33			Ü
Lack-	10	4.60	0.46	3.68	0.062	Not
of-fit						Significant
Pure error	6	0.75	0.12			
Total	30	1788.14				
R ² R ² -adj	99.70% 99.44%		R ² (pred) SD	98.46% 0.58		

The influence of reaction time and methanol to PFAD molar ratio were investigated by varying reaction time from 1 to 5 h and molar ratio from 9:1 to 21:1, as displayed in Fig. 5e. Esterification is a reversible reaction that requires longer reaction time and higher molar ratios of

methanol to PFAD to shift the reaction toward the products by providing sufficient time for methanol to form methoxide groups and interact with fatty acids to diffuse onto the catalyst active sites and produce FAME [61]. The yield increased from 80% to >86% from 1 to 3.8 h at molar ratios of 9:1 to 18:1. Yield gradually decreased when the reaction time was increased to 5 h and higher methanol to PFAD molar ratios (>18:1) due to methanol flooding on the catalyst surface that prevented fatty acid protonation [62].

Considering the results of the RSM-CCD procedure and significant variables that affected biodiesel yield, certain levels of input parameters were selected. The RSM-CCD model estimated that an optimized yield of 99.42% could be achieved at reaction conditions of 75 $^{\circ}$ C, 1.3 h, 4.2 wt% catalyst, and a molar ratio of methanol to PFAD of 21:1. The theoretical prediction was validated experimentally in triplicate under the optimized conditions to provide an average yield of 98.6%.

3.8. Plausible esterification mechanism of UiO-66/SO₃H

The esterification of PFAD was catalyzed by the sulfonated UiO-66 catalyst, as shown in the proposed mechanism in Fig. 6. The reaction was initiated by deprotonation of a $-SO_3H$ group after interaction with an oxygen atom from a fatty acid carbonyl group, leading to new bond formation between the free proton and the electrophilic carbon of the carbonyl group. The protonated carbon then underwent a nucleophilic attack by methanol, followed by proton transfer from methanol to one of the hydroxyl (-OH) groups of the fatty acid intermediate. Subsequently, water was released to form the FAME after a few steps of rearrangement. Finally, the ester was deprotonated to release a proton that was free to react with another PFAD fatty acid, thereby perpetuating the process.

3.9. Catalyst reusability and deactivation analysis

The UiO-66/SO₃H catalyst was recovered and reused for eight consecutive esterification cycles. The properties of the reused sample were studied, as shown in Fig. 7 and Table 7. The reusability tests

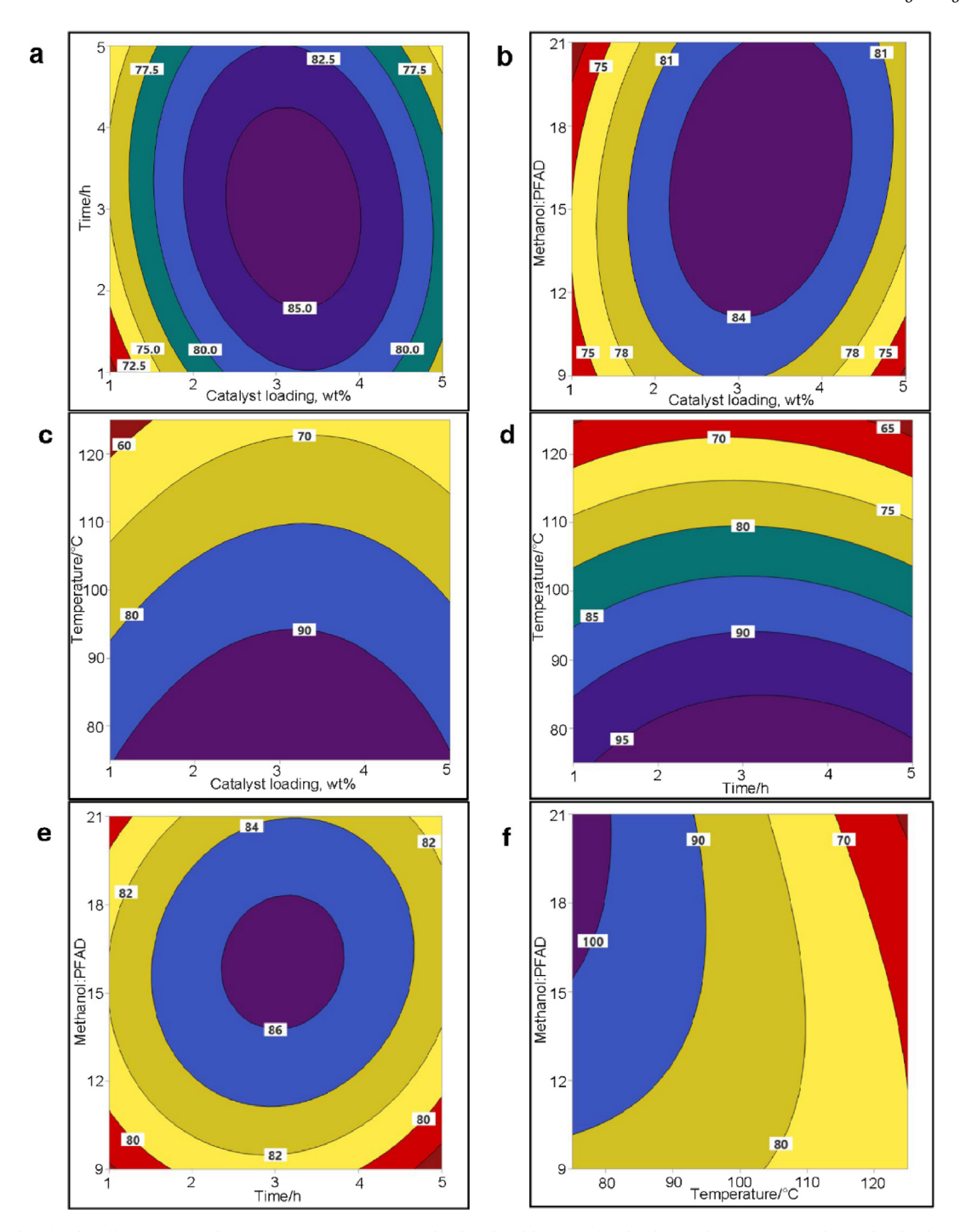


Fig. 5. Contour plots for the effect of various binary reaction parameters on biodiesel yield: (a) catalyst loading and reaction time, (b) catalyst loading and methanol to PFAD molar ratio, (c) catalyst loading and reaction temperature, (d) time and temperature, (e) time and methanol to PFAD molar ratio, and (f) temperature and methanol to PFAD molar ratio.

demonstrated that catalytic esterification by UiO-66/SO $_3$ H was efficient for seven reaction cycles with yields of > 70%, but yield dropped to 53% during the eighth cycle (Fig. 7a). The yield reduction was due to the loss of active sites by deposition of unreacted fatty acids, excess methanol, and biodiesel on the active pores [63]. The analysis of textural and absorption measurements of surface area and total acidity were reduced from 503.02 to 276.04 m 2 /g and 7.89 to 1.46 mmol/g, respectively, after the eighth catalytic cycle (Table 7, Fig. 7b and c), indicating that the pores were covered by reactants. The active pores blockage by these contaminants caused N $_2$ adsorption and NH $_3$ absorption to reduce their

affinity for textural [51,52] and acidity measurement [64], which literally led to ineffective catalytic activity. In Fig. 7d, the infrared absorption of spent UiO-66/SO $_3$ H catalyst clearly exhibited two additional bands corresponding to aliphatic -C-H-H stretching [65], recorded at 2916 cm $^{-1}$ and 2858 cm $^{-1}$, confirming the presence of unreacted fatty acids and biodiesel on the catalyst surface. Meanwhile the other functional groups remained unchanged, aside from a slight shift and reduction in intensity particularly in the symmetrical stretching absorption bands of SO $_3$ and O=S=O at 1108 cm $^{-1}$ and 1024 cm $^{-1}$ [66], respectively. This change is possibly due to the overlapping absorption of

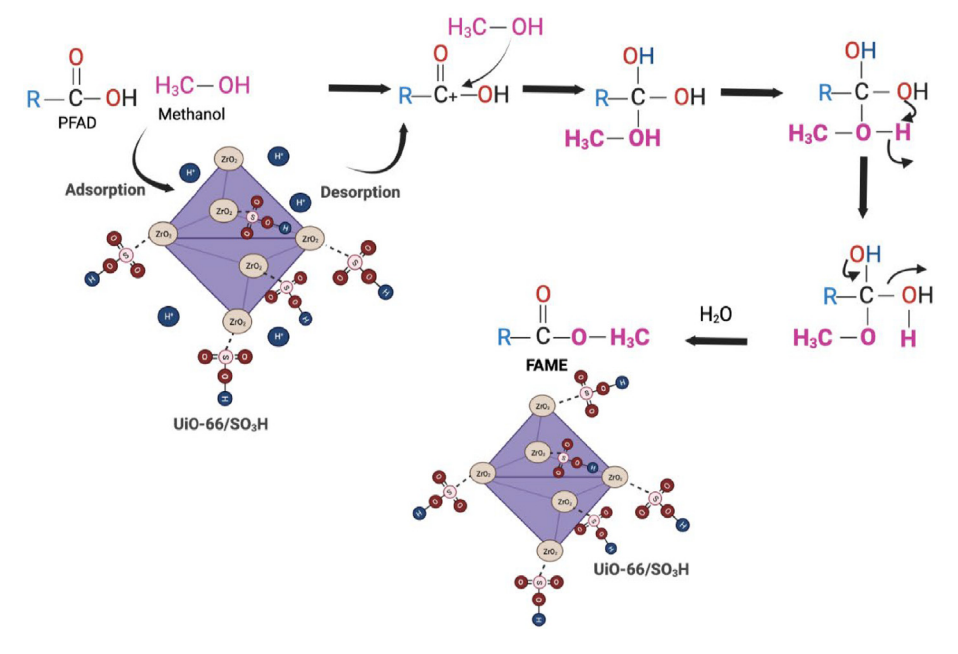


Fig. 6. Proposed mechanism of biodiesel production from PFAD and methanol using acidic UiO-66/SO₃H.

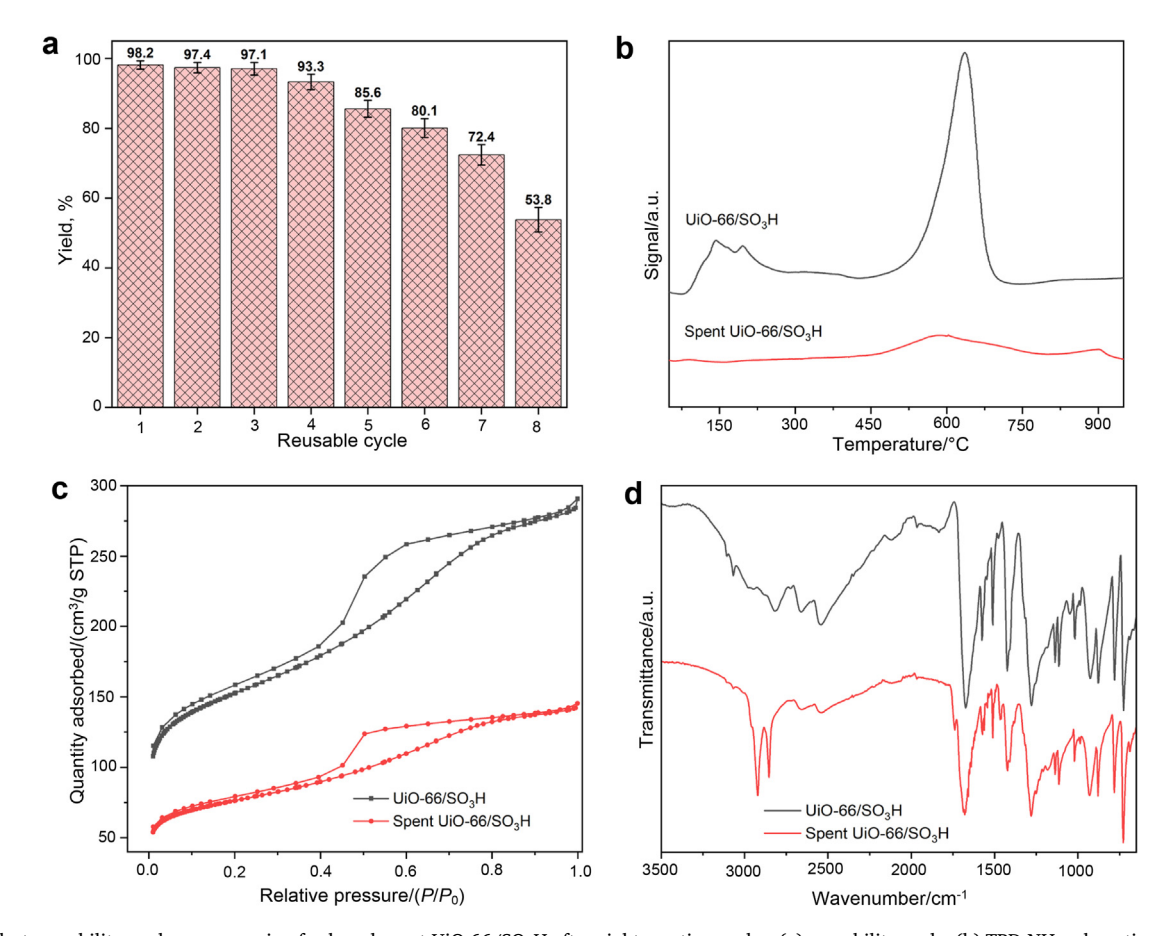


Fig. 7. Catalyst reusability analyses comparing fresh and spent UiO-66/SO₃H after eight reaction cycles: (a) reusability cycle, (b) TPD-NH₃ adsorption peaks, (c) BET adsorption-desorption, and (d) infrared absorption analysis.

contaminants masked on the spent catalyst porous surface compared to fresh $UiO-66/SO_3H$. Thus, the reduction of available active sites reduced the mass transfer activity of methanol and fatty acids for esterification and lowered biodiesel yield [67].

3.10. Comparison of catalytic performance with reported UiO-66-based catalysts

Table 8 summarizes the comparative evaluation of the esterification performances of UiO-66 based catalysts for the reported and current

Table 7Surface properties of pristine and spent UiO-66/SO₃H after eight reaction cycles.

Catalyst	Surface area/ (m ² /g)	Pore diameter/ nm	Total absorption NH ₃ / (mmol/g)
UiO-66/SO₃H	503.02	3.30	7.98
Spent UiO-66/	276.04	2.00	1.46
SO-H			

work. In this study, functionalized UiO-66 (UiO-66/SO₃H) demonstrated efficient catalytic esterification of PFAD, achieving a maximum yield of 98.2% at a lower reaction temperature within a reaction time of less than 2 h, with less catalyst consumption. In addition, the UiO-66/SO₃H catalyst possesses a high acidic density (7.98 mmol/g), which makes it highly catalytically selective for the conversion of PFAD into FAME with better mechanical stability to sustain up to 8 reaction cycles. In comparison with other reported UiO-66-based catalysts, most of these reactions only esterified a single type of fatty acid with longer reaction times, higher reaction temperatures, high catalyst loadings, and high volumes of methanol. In conclusion, the UiO-66/SO₂H catalyst investigated in the present study demonstrated superior performance with respect to acid density, reaction conditions, yield, catalyst efficiency, and reusability compared to similar catalysts reported in the literature [68-73]. Thus, the UiO-66/SO₃H catalyst synthesized in the present study warrants further investigation as a viable option for large-scale biodiesel production.

3.11. LCA results of the production of biodiesel from PFAD

Fig. 8 presents the comprehensive outcomes of our LCA, encompassing seven distinct environmental impact categories and examining three different classifications for PFAD. Notably, the assessment reveals that the global warming impact, quantified in kilograms of $\rm CO_2$ equivalent (kg $\rm CO_2$ eq) emissions, varies significantly depending on the classification of PFAD: 5.71 kg $\rm CO_2$ eq when considered a residue, 5.79 kg $\rm CO_2$ eq as a byproduct, and 6.68 kg $\rm CO_2$ eq when categorized as a coproduct. Among these environmental categories, it becomes evident that electricity exhibits the most substantial influence on global warming, accounting for 55.24%–64.60% of $\rm CO_2$ equivalent emissions.

Regarding terrestrial ecotoxicity, which measures impacts on kilograms of 1,4-dichlorobenzene (1,4-DCB) equivalent (kg 1,4-DCB eq), we obtained values of 3.24, 3.44, and 5.82 kg 1,4-DCB eq for the residue, byproduct, and coproduct classifications of PFAD, respectively. Notably, when PFAD is considered as a coproduct, the primary contributors to terrestrial ecotoxicity are methanol and PFAD. Interestingly, fossil resource scarcity appears relatively unaffected by PFAD classification, with methanol and electricity accounting for over 90% of the total impacts in this category.

An intriguing finding is that, in most environmental impact categories, water plays a minor role, with methanol emerging as a prominent contributor. Particularly noteworthy is the substantial impact of PFAD when classified as a coproduct in the palm oil refining process, as it contributes over 40% of impacts related to stratospheric ozone depletion, terrestrial ecotoxicity, freshwater ecotoxicity, and marine ecotoxicity. These findings underscore the importance of considering PFAD classification in the context of sustainable biodiesel production.

A comparative analysis of our LCA results was conducted, specifically focusing on two critical environmental impact categories: global warming potential and acidification potential. For the sake of meaningful comparison, we standardized the functional unit at 1 MJ of biodiesel. Notably, we categorized PFAD as a byproduct arising from the production of RPO. The outcomes of this comparative evaluation are presented in Table 9 and illustrated in Fig. 9. Our study revealed that while the acidification potential remained relatively low, the global warming potential was the largest, apart from cases involving microalgae-based biodiesel production.

Table 8
List of current and reported UiO-66-based catalysts in preforming catalytic esterification of biodiesel.

Catalyst	Biodiesel feedstock	Acid density/ (mmol/g)	Reaction parameters (Methanol: oil, catalyst loading, reaction time, temperature) (Yield,%)	Reusability	Ref.
UiO-66/ SO ₃ H	PFAD	7.98	21:1, 4.2 wt %, 1.3 h, 75 °C (98.2%)	8	Current study
UiO-66- 100 °C	Tributyrin	1.16	52:1, 9 wt%, 5 h, 120 °C (96.0%)	4	[68]
UiO-66	Lauric acid	_	26:1, 8 wt%, 2 h, 60 °C (94%)	-	[69]
UiO-66- SO ₃ H	Oleic acid	_	9:1, 6 wt%, 3 h, 80 °C (85.0%)	4	[70]
UiO-66/SA	Oleic acid	1.40	21.9:1, 7.6 wt %, 1.8 h, 85 °C (94.4%)	5	[71]
FDCA/SA- UiO- 66(Zr)	Oleic acid	0.06	39.1:1, 6.1 wt %, 60.2 °C, 24.5 h (98.4%)	6	[72]
PTSA@UiO- 66(Zr)	Oleic acid	0.18	12:1, 8 wt%, 2 h, 70 °C (91.3%)	4	[73]

Furthermore, a sensitivity analysis was employed to pinpoint the pivotal parameters influencing our study. To gain a deeper understanding of these parameters' effects, we systematically altered their values within a range of $\pm 30\%$ while maintaining all other factors constant. The outcomes of this sensitivity analysis were depicted in Fig. 10. Our findings revealed that when manipulating input variables, electricity emerged as the most influential factor, exerting the most significant impact. In contrast, the influence of water on global warming potential remained minimal and almost imperceptible. On the other hand, when assessing acidification potential, it was evident that altering the quantity of methanol was the primary driver of change, with water exerting a relatively minor influence.

From the perspective of ACP, PFAD with the catalyst in this study exhibits potential compared to other feedstocks. Through the environmental assessment and sensitivity analysis conducted in this study, it was found that the environmental impact due to electricity consumption is significant. If process optimization regarding electricity consumption is achieved, the process of producing biodiesel using the catalyst developed in this study is expected to be environmentally competitive against other feedstocks. In addition to environmental assessment of biodiesel production using emerging technologies, economic benefits are also a crucial method for evaluating the feasibility of industrial application [26]. PFAD have typically higher economic potentials in the biofuel sector compared to palm oil [85,86]. If process optimization can be achieved and the biodiesel production process using PFAD and the catalyst from this study can secure environmental competitiveness, it would then be appropriate to analyze the economic viability to assess the feasibility of actual industrial application.

4. Conclusions

We successfully designed and prepared an acid-functionalized (-SO₃H) heterogeneous UiO-66 MOF nanocatalyst for the esterification of PFAD into biodiesel. Sulfonation of pristine UiO-66 afforded UiO-66/SO₃H with high acidity, surface area, and thermal stability. Both pristine

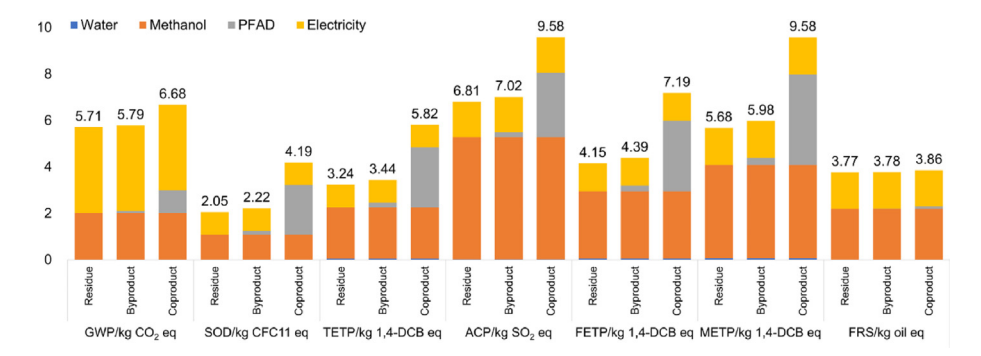


Fig. 8. Environmental impacts of the production biodiesel in this study for assuming PFAD as residue, byproduct, and coproduct. Each environmental impact is calculated based on the functional unit of 1 kg of biodiesel. (GWP: Global warming potential, SOD: Stratospheric ozone depletion, ACP: Acidification potential, TETP: Terrestrial ecotoxicity, FETP: Freshwater ecotoxicity, METP: Marine ecotoxicity, and FRW: Fossil resource scarcity).

Table 9
Comparison of PFAD LCA data with other biodiesel studies based on 1 MJ of biodiesel.

Feedstock	Global warming potential/(kg CO ₂ eq/MJ biodiesel)	Acidification potential/(kg SO ₂ eq/ MJ biodiesel)	Ref.
PFAD (as byproduct)	0.1523	1.847E-04	Present study
Lignocellulosic biomass (lignin-rich stream) ^a	0.0561	3.800E-04	[74]
Lignocellulosic biomass (corn stover) ^a	0.0584	4.860E-04	[74]
Palm oil ₁ ^a	0.0031	5.210E-05	[75]
Palm oil ₂ ^a , ^b	0.0018	8.833E-05	[75,76]
Palm oil ₃ ^a , ^b	0.0052	1.054E-04	[75,77]
Palm oil ₄ ^a , ^b	0.0033	5.773E-05	[75,78]
Palm oil ₅ ^a , ^b	0.0129	2.014E-04	[75,79]
Palm oil ₆ c	0.0344	5.500E-05	[80]
Soybean ^c	0.1364	3.485E-04	[81]
Used cooking oil ^c	0.0135	1.346E-04	[82]
Estuarine microalgae ^c	0.0207	1.429E-04	[81]
Microalgae ₁ ^a	5.74	2.640E-02	[83]
Microalgae2ª	3.62	$4.160E-02^{d}$	[84]

^a Data taken directly from the original studies.

UiO-66 and UiO-66/SO₃H possessed micro-mesoporous crystalline structures with high surface areas. As anticipated, the acidity of the sulfonated material was higher than the pristine precursor. The catalytic activity of UiO-66/SO₃H was verified by the esterification of PFAD with methanol to produce FAME (biodiesel). The effects and interactions among the reaction parameters on yield were examined and optimized by RSM-CCD. Yield prediction by RSM and experimental yields were in close agreement. A yield of 98.6% was attained under optimized reaction conditions. Reusability experiments showed that the catalyst was active for seven cycles with an average yield of 72.4%, but the yield decreased to 53.8% after the eighth cycle. Analysis of spent catalyst revealed that active sites were lost due to deposition of reactants and FAME on the surface, thus explaining the cause of yield reduction. These results indicated that the acidic MOF catalyst is useful for biodiesel production. In the context of categorizing PFAD as a byproduct, our research identified a global warming potential of 5.79 kg CO₂ eq and an acidification potential of 7.02E-03 kg of SO₂ eq. Further exploration through sensitivity analysis

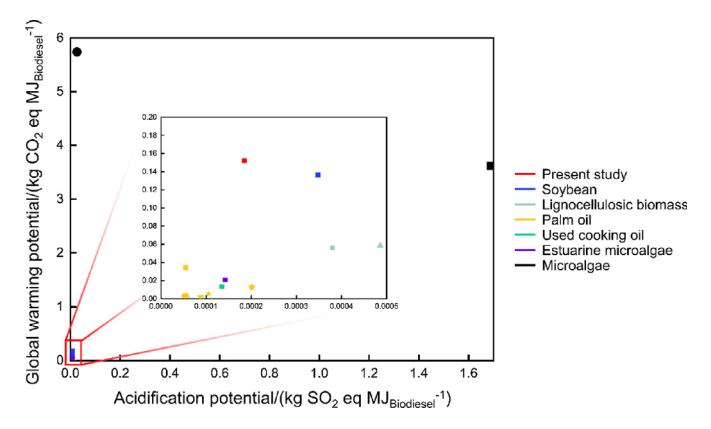


Fig. 9. The comparison of global warming potential and acidification potential with other biodiesel studies based on 1 MJ of biodiesel.

elucidated the dominant drivers of these environmental impacts, revealing that electricity prominently influenced global warming potential while methanol played a pivotal role in affecting acidification potential. This research thus revealed a new heterogeneous catalyst for production of biodiesel from inexpensive, low-quality feedstocks. Future work will be directed at lowering reaction conditions and increasing catalyst reusability to further improve process economics and environmental impact.

Data availability

Data will be made available on request.

CRediT authorship contribution statement

Balkis Hazmi: Writing original draft, Software, Investigation, Formal analysis, Data curation. Umer Rashid: Writing review & editing, Visualization, Validation, Supervision, Software, Project administration, Methodology, Funding acquisition, Formal analysis, Conceptualization. Bryan R. Moser: Writing review & editing, Validation, Methodology. Mohd Hafizuddin Ab Ghani: Writing original draft, Validation, Investigation, Data curation. Fahad A. Alharthi: Writing review & editing, Validation, Resources, Investigation, Data curation. Jeehoon Han: Writing review & editing, Validation, Project administration, Methodology, Investigation, Formal analysis, Data curation, Conceptualization. Jiyun Yoo: Writing original draft, Validation, Formal analysis, Data curation.

^b Sourced from a study by Rocha et al. [75], based on the inventory data presented in the individual references.

^c Based on a functional unit of kg of biodiesel as presented in the respective references, converted to 1 MJ of biodiesel.

 $^{^{}m d}$ Converted to kg SO₂ eq based on mol H * eq as presented in Soratana et al. [84].

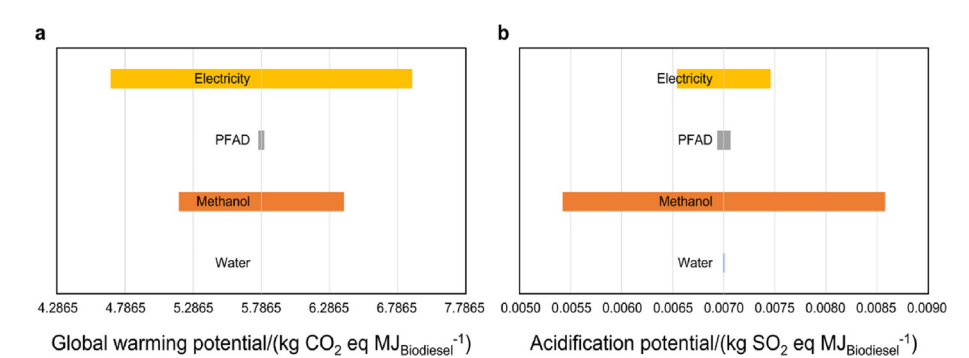


Fig. 10. Sensitivity analysis for biodiesel production in terms of (a) global warming potential and (b) acidification potential.

Disclaimer

Mention of trade names or commercial products in this publication is solely for the purpose of providing specific information and does not imply recommendation or endorsement by the U.S. Department of Agriculture. USDA is an equal opportunity provider and employer.

Declaration of competing interests

The authors declare that they have no known competing financial interests or personal relationships that could have appeared to influence the work reported in this paper.

Acknowledgements

This research work obtained financial support under Insiatif Putra Siswazah from Universiti Putra Malaysia (Kod Project: 9774800). Authors extend their thanks to Researchers Supporting Project (RSP2025R160), King Saud University (Riyadh, Saudi Arabia). This research was funded in part by the U.S. Department of Agriculture, Agricultural Research Service.

Appendix A. Supplementary data

Supplementary data to this article can be found online at https://doi.org/10.1016/j.gce.2024.10.001.

References

- [1] A.H. Al-Muhtaseb, F. Jamil, L. Al-Haj, M.A. Al-Hinai, M. Baawain, M.T.Z. Myint, D. Rooney, Efficient utilization of waste date pits for the synthesis of green diesel and jet fuel fractions, Energy Convers. Manag. 127 (2016) 226–232.
- [2] P. Rechnia-gor, A. Malaika, P. Rechnia-Goracy, A. Malaika, M. Kozłowski, Acidic activated carbons as catalysts of biodiesel formation, Diam. Relat. Mater. 87 (2018) 124–133.
- [3] N. Mansir, S. Hwa Teo, M. Lokman Ibrahim, T.Y. Yun Hin, Synthesis and application of waste eggshell derived CaO supported W-Mo mixed oxide catalysts for FAME production from waste cooking oil: effect of stoichiometry, Energy Convers. Manag. 151 (2017) 216–226.
- [4] Y.-M. Dai, K.-T. Chen, P.-H. Wang, C.-C. Chen, Solid-base catalysts for biodiesel production by using silica in agricultural wastes and lithium carbonate, Adv. Powder Technol. 27 (2016) 2432–2438.
- [5] M. Alsharifi, H. Znad, S. Hena, M. Ang, Biodiesel production from canola oil using novel Li/TiO₂ as a heterogeneous catalyst prepared *via* impregnation method, Renew. Energy 114 (2017) 1077–1089.
- [6] K. Fiala, A. Thongiarad, R. Leesing, Valorization of durian peel as a carbon feedstock for a sustainable production of heterogeneous base catalyst, single cell oil and yeast-based biodiesel. Carbon Resour. Conver. 7 (2024) 100224.
- [7] J. Huang, T. Liu, K. Wang, Z. Huang, J. Wang, S.L. Rokhum, H. Li, Room-temperature and carbon-negative production of biodiesel via synergy of geminal-atom and photothermal catalysis, Environ. Chem. Lett. 22 (2024) 1607–1613.
- [8] Y. Li, K. Zhu, Y. Jiang, L. Chen, H. Zhang, H. Li, S. Yang, Biomass-derived hydrophobic metal-organic frameworks solid acid for green efficient catalytic esterification of oleic acid at low temperatures, Fuel Process. Technol. 239 (2023) 107558.
- [9] S.E.M. Elhenawy, M. Khraisheh, F. Almomani, G. Walker, Metal-organic frameworks as a platform for CO₂ capture and chemical processes: adsorption,

- membrane separation, catalytic-conversion, and electrochemical reduction of CO_2 , Catalysts 10 (2020) 1293.
- [10] H. Zhou, H. Wang, C. Yue, L. He, H. Li, H. Zhang, S. Yang, T. Ma, Photocatalytic degradation by TiO₂-conjugated/coordination polymer heterojunction: preparation, mechanisms, and prospects, Appl. Catal. B 344 (2024) 123605.
- [11] A. Nikseresht, A. Daniyali, M. Ali-Mohammadi, A. Afzalinia, A. Mirzaie, Ultrasound-assisted biodiesel production by a novel composite of Fe(III)-based MOF and phosphotangestic acid as efficient and reusable catalyst, Ultrason. Sonochem. 37 (2017) 203–207.
- [12] J. Chen, W. Yan, E.J. Townsend, J. Feng, L. Pan, V. Del Angel Hernandez, C.F.J. Faul, Tunable surface area, porosity, and function in conjugated microporous polymers, Angew. Chem. 131 (2019) 11841–11845.
- [13] F. Liu, X. Ma, H. Li, Y. Wang, P. Cui, M. Guo, H. Yaxin, W. Lu, S. Zhou, M. Yu, Dilute sulfonic acid post functionalized metal organic framework as a heterogeneous acid catalyst for esterification to produce biodiesel, Fuel 266 (2020) 117149.
- [14] H. Guo, J. Cheng, Y. Mao, L. Qian, Y. Shao, X. Yang, W. Yang, Acid-base bifunctional catalyst with coordinatively unsaturated cobalt-nitrogen sites for the simultaneous conversion of microalgal triglycerides and free fatty acids into biodiesel, Bioresour. Technol. 350 (2022) 126862.
- [15] A. Ghorbani-Choghamarani, Z. Taherinia, Y.A. Tyula, Efficient biodiesel production from oleic and palmitic acid using a novel molybdenum metal-organic framework as efficient and reusable catalyst, Sci. Rep. 12 (2022) 10338.
- [16] W. Liu, F. Wang, P. Meng, S.-Q. Zang, Sulfonic acids supported on UiO-66 as heterogeneous catalysts for the esterification of fatty acids for biodiesel production, Catalysts 10 (2020) 1271.
- [17] N. Mulik, V. Bokade, Immobilization of HPW on UiO-66-NH₂ MOF as efficient catalyst for synthesis of furfuryl ether and alkyl levulinate as biofuel, Mol. Catal. 531 (2022) 112689.
- [18] T. Ma, D.B. Liu, Z.X. Liu, J. Xu, Y. Dong, G. Chen, Z. Yun, 12-Tungstophosphoric acid-encapsulated metal-organic framework UiO-66: a promising catalyst for the esterification of acetic acid with n-butanol, J. Taiwan Inst. Chem. Eng. 133 (2022), 104277–104277.
- [19] B.O. Yusuf, S.A. Oladepo, S.A. Ganiyu, A.M.P. Peedikakkal, Synthesis and evaluation of CuO/UiO-66 metal-organic frameworks as a solid catalyst for biodiesel production from waste cooking oil, Mol. Catal. 564 (2024) 114313.
- [20] S.P. Gouda, J.M. Jasha, P. Kumar, A. Dhakshinamoorthy, U. Rashid, S.L. Rokhum, Microwave-assisted biodiesel production using UiO-66 MOF derived nanocatalyst: process optimization using response surface methodology, Catalysts 12 (2022) 1312
- [21] A. Inayat, C. Ghenai, D. Hammad, S. Almarzooqi, R. Tariq, F. Jamil, A. Bokhari, M. Ayoub, Optimization of biodiesel production from neem oil using KOH supported with activated carbon, Chem. Eng. Trans. 81 (2020) 1051–1056.
- [22] M.D.G. de Luna, J.L. Cuasay, N.C. Tolosa, T.W. Chung, Transesterification of soybean oil using a novel heterogeneous base catalyst: synthesis and characterization of Na-pumice catalyst, optimization of transesterification conditions, studies on reaction kinetics and catalyst reusability, Fuel 209 (2017) 246–253.
- [23] B. Maleki, S.S. Ashraf Talesh, Sustainable biodiesel production from wild oak (Quercus brantii Lindl) oil as a novel and potential feedstock via highly efficient Co@ CuO nanocatalyst: RSM optimization and CI engine assessment, Renew. Energy 224 (2024) 120127.
- [24] L. He, L. Chen, Y. Nie, M. He, G. Wu, Y. Li, H. Tian, H. Zhang, A practical approach for enhanced biodiesel production using organic modified montmorillonites as efficient heterogeneous hybrid catalysts, Green Chem. 26 (2024) 5954–5965.
- [25] B. Zheng, L. Ban, Y. Nie, L. Chen, S. Yang, H. Zhang, Sustainable production of biodiesel enabled by acid-base bifunctional ZnF₂ via one-pot transformation of Koelreuteria integrifoliola oil: process optimization, kinetics study and cost analysis, J. Clean, Prod. 453 (2024) 142263.
- [26] N. Rajendran, D. Kang, J. Han, B. Gurunathan, Process optimization, economic and environmental analysis of biodiesel production from food waste using a citrus fruit peel biochar catalyst, J. Clean. Prod. 365 (2022) 132712.
- [27] Z.L. Chung, Y.H. Tan, Y.S. Chan, J. Kansedo, N.M. Mubarak, M. Ghasemi, M.O. Abdullah, Life cycle assessment of waste cooking oil for biodiesel production using waste chicken eggshell derived CaO as catalyst via transesterification, Biocatal. Agric. Biotechnol. 21 (2019) 101317.

- [28] D. Mu, C. Xin, W. Zhou, Life cycle assessment and techno-economic analysis of algal biofuel production, in: A. yousaf (Ed.), Microalgae Cultivation for Biofuels Production, Elsevier, 2020, pp. 281–292. Bangladesh.
- [29] J. Huang, J. Wang, Z. Huang, T. Liu, H. Li, Photothermal technique-enabled ambient production of microalgae biodiesel: mechanism and life cycle assessment, Bioresour. Technol. 369 (2023) 128390.
- [30] J. Byun, J. Han, Sustainable development of biorefineries: integrated assessment method for co-production pathways, Energy Environ. Sci. 13 (2020) 2233–2242.
- [31] J. Byun, O. Kwon, H. Park, J. Han, Food waste valorization to green energy vehicles: sustainability assessment, Energy Environ. Sci. 14 (2021) 3651–3663.
- [32] H. Xu, U. Lee, M. Wang, Life-cycle energy use and greenhouse gas emissions of palm fatty acid distillate derived renewable diesel, Renew. Sustain. Energy Rev. 134 (2020) 110144.
- [33] W. Xie, F. Wan, Immobilization of polyoxometalate-based sulfonated ionic liquids on UiO-66-2COOH metal-organic frameworks for biodiesel production via one-pot transesterification-esterification of acidic vegetable oils, Chem. Eng. J. 365 (2019) 40.50
- [34] H. Jiang, C. Xue, W. Sun, Z. Gong, X. Yuan, Acid regulation of defective sulfonicacid-functionalized UiO-66 in the esterification of cyclohexene with formic acid, Catal. Lett. 153 (2023) 836–849.
- [35] S.E. Moradi, A.M.H. Shabani, S. Dadfarnia, S. Emami, Sulfonated metal organic framework loaded on iron oxide nanoparticles as a new sorbent for the magnetic solid phase extraction of cadmium from environmental water samples, Anal. Methods 8 (2016) 6337–6346.
- [36] Z. Ma, X. Xing, Z. Qu, Y. Sun, G. Sun, X. Wang, Y. Han, Activity of microporous lignin-derived carbon-based solid catalysts used in biodiesel production, Int. J. Biol. Macromol. 164 (2020) 1840–1846.
- [37] B. Hazmi, U. Rashid, S. Kawi, W.N.A.W. Mokhtar, T.C.S. Yaw, B.R. Moser, A. Alsalme, Palm fatty acid distillate esterification using synthesized heterogeneous sulfonated carbon catalyst from plastic waste: characterization, catalytic efficacy and stability, and fuel properties, Process Saf. Environ. Protect. 162 (2022) 1139–1151.
- [38] R.R.C. Bastos, A.P. da Luz Corr\u00e9a, P.T.S. da Luz, G.N. da Rocha Filho, J.R. Zamian, L.R.V. da Concei\u00e7\u00e3o, Optimization of biodiesel production using sulfonated carbonbased catalyst from an amazon agro-industrial waste, Energy Convers. Manag. 205 (2020) 112457.
- [39] F.T. Alshorifi, D.E. Tobbala, S.M. El-Bahy, M.A. Nassan, R.S. Salama, The role of phosphotungstic acid in enhancing the catalytic performance of UiO-66 (Zr) and its applications as an efficient solid acid catalyst for coumarins and dihydropyrimidinones synthesis, Catal. Commun. 169 (2022) 106479.
- [40] Q. Zhang, D. Lei, Q. Luo, J. Wang, T. Deng, Y. Zhang, P. Ma, Efficient biodiesel production from oleic acid using metal-organic framework encapsulated Zr-doped polyoxometalate nano-hybrids, RSC Adv. 10 (2020) 8766–8772.
- [41] R. Bardestani, G.S. Patience, S. Kaliaguine, Experimental methods in chemical engineering: specific surface area and pore size distribution measurements—BET, BJH, and DFT, Can. J. Chem. Eng. 97 (2019) 2781–2791.
- [42] R. Soltani, R. Pelalak, M. Pishnamazi, A. Marjani, S.M. Sarkar, A.B. Albadarin, S. Shirazian, Novel bimodal micro-mesoporous Ni₅₀Co₅₀-LDH/UiO-66-NH₂ nanocomposite for Tl(I) adsorption, Arab. J. Chem. 14 (2021) 103058.
- [43] D. Tang, M. Yin, X. Du, Y. Duan, J. Chen, T. Qiu, Wettability tunable conjugated microporous poly(aniline)s for long-term, rapid and ppb level sequestration of Hg(II), Chem. Eng. J. 474 (2023) 145527.
- [44] R.F. Abdullah, U. Rashid, Y.H. Taufiq-Yap, M.L. Ibrahim, C. Ngamcharussrivichai, M. Azam, Synthesis of bifunctional nanocatalyst from waste palm kernel shell and its application for biodiesel production, RSC Adv. 10 (2020) 27183–27193.
- [45] Y.T. Wang, X.X. Yang, J. Xu, H.L. Wang, Z.B. Wang, L. Zhang, S.L. Wang, J.L. Liang, Biodiesel production from esterification of oleic acid by a sulfonated magnetic solid acid catalyst, Renew. Energy 139 (2019) 688–695.
- [46] F.G. Cirujano, A. Dhakshinamoorthy, Engineering of active sites in metal-organic frameworks for biodiesel production, Adv. Sustain. Syst. 5 (2021) 2100101.
- [47] Q. Zhang, X. Yang, J. Yao, J. Cheng, Bimetallic MOF-Derived synthesis of cobalt-cerium oxide supported phosphotungstic acid composites for the oleic acid esterification, J. Chem. 2021 (2021) 2131960.
- [48] S. Chellappan, V. Nair, V. Sajith, K. Aparna, Experimental validation of biochar based green Bronsted acid catalysts for simultaneous esterification and transesterification in biodiesel production, Bioresour. Technol. Rep. 2 (2018) 38.444
- [49] L. Peng, A. Bahadoran, S. Sheidaei, P. Joolaei Ahranjani, H. Kamyab, B. Oryani, S. Sadia Arain, S. Rezania, Magnetic graphene oxide supported tin oxide (SnO) nanocomposite as a heterogeneous catalyst for biodiesel production from soybean oil, Renew. Energy 224 (2024) 120050.
- [50] R. D'Souza, T. Vats, A. Chattree, P.F. Siril, Graphene supported magnetically separable solid acid catalyst for the single step conversion of waste cooking oil to biodiesel, Renew. Energy 126 (2018) 1064–1073.
- [51] X. Lou, D. Tang, C. Ye, J. Chen, T. Qiu, Conjugated micro-mesoporous poly(aniline)s for ultrafast Hg (II) capture, Sep. Purif. Technol. 325 (2023) 124616.
- [52] X. Ye, X. Chen, D. Chen, Z. Qian, Y. Duan, X. Du, C. Lin, J. Chen, W. Luo, Unconventional extraction of uranium from seawater through microenvironmentspecific conjugated microporous poly(aniline)s, Sep. Purif. Technol. 353 (2025) 128362...
- [53] O.N. Syazwani, U. Rashid, M.S. Mastuli, Y.H. Taufiq-Yap, Esterification of palm fatty acid distillate (PFAD) to biodiesel using Bi-functional catalyst synthesized from waste angel wing shell (*Cyrtopleura costata*), Renew. Energy 131 (2019) 187–196.

- [54] S.-I.I. Akinfalabi, U. Rashid, R. Yunus, Y.H. Taufiq-Yap, Synthesis of biodiesel from palm fatty acid distillate using sulfonated palm seed cake catalyst, Renew. Energy 111 (2017) 611–619.
- [55] T. Tamoradi, A.R. Kiasat, H. Veisi, V. Nobakht, Z. Besharati, B. Karmakar, MgO doped magnetic graphene derivative as a competent heterogeneous catalyst producing biofuels via transesterification: process optimization through response surface methodology (RSM), J. Environ. Chem. Eng. 9 (2021) 106009.
- [56] F.H. Alhassan, U. Rashid, Y.H. Taufiq-Yap, Synthesis of waste cooking oil-based biodiesel via effectual recyclable bi-functional Fe₂O₃MnOSO₄²/ZrO₂ nanoparticle solid catalyst, Fuel 142 (2015) 38–45.
- [57] A.N. Amenaghawon, K. Obahiagbon, V. Isesele, F. Usman, Optimized biodiesel production from waste cooking oil using a functionalized bio-based heterogeneous catalyst, Clean Eng. Technol. 8 (2022) 100501.
- [58] L. Guo, W. Xie, C. Gao, Heterogeneous H₆PV₃MoW₈O₄₀/AC-Ag catalyst for biodiesel production: preparation, characterization and catalytic performance, Fuel 316 (2022) 123352.
- [59] B. Maleki, B. Singh, H. Eamaeili, Y.K. Venkatesh, S.S.A. Talesh, S. Seetharaman, Transesterification of waste cooking oil to biodiesel by walnut shell/sawdust as a novel, low-cost and green heterogeneous catalyst: optimization via RSM and ANN, Ind. Crops Prod. 193 (2023) 116261.
- [60] G. Baskar, A. Gurugulladevi, T. Nishanthini, R. Aiswarya, K. Tamilarasan, Optimization and kinetics of biodiesel production from Mahua oil using manganese doped zinc oxide nanocatalyst, Renew. Energy 103 (2017) 641–646.
- [61] N. Hindryawati, G. Pragas, R. Karim, K. Feng, Transesterification of used cooking oil over alkali metal (Li, Na, K) supported rice husk silica as potential solid base catalyst, Eng. Sci. Technol. Inter. J. 17 (2014) 95–103.
- [62] D.N. Faria, D.F. Cipriano, M.A. Schettino, Á.C. Neto, A.G. Cunha, J.C.C. Freitas, Na,Ca-based catalysts supported on activated carbon for synthesis of biodiesel from soybean oil, Mater. Chem. Phys. 249 (2020) 123173.
- [63] E.O. Ajala, M.A. Ajala, A.O. Ajao, H.B. Saka, A.C. Oladipo, Calcium-carbide residue: a precursor for the synthesis of CaO-Al₂O₃-SiO₂-CaSO₄ solid acid catalyst for biodiesel production using waste lard, Chem. Eng. J. Adv. 4 (2020) 100033.
- [64] R.O. Araujo, V.O. Santos, F.C.P. Ribeiro, J. da S. Chaar, A.M. Pereira, N.P.S. Falcão, L.K.C. de Souza, Magnetic acid catalyst produced from acai seeds and red mud for biofuel production, Energy Convers. Manag. 228 (2021) 113636.
- [65] A.N. Gutiérrez-López, V.Y. Mena-Cervantes, S.M. García-Solares, J. Vazquez-Arenas, R. Hernández-Altamirano, NaFeTiO₄/Fe₂O₃–FeTiO₃ as heterogeneous catalyst towards a cleaner and sustainable biodiesel production from *Jatropha curcas* L. oil, J. Clean. Prod. 304 (2021) 127106.
- [66] G.M.A. Bureros, A.A. Tanjay, D.E.S. Cuizon, A.W. Go, L.K. Cabatingan, R.C. Agapay, Y.H. Ju, Cacao shell-derived solid acid catalyst for esterification of oleic acid with methanol. Renew. Energy 138 (2019) 489–501.
- [67] C.V. Satyanarayana, D. Srikant, H.R. Gurav, Catalyst deactivation and regeneration, in: S.S. Joshi, V.V. Ranade (Eds.), Industrial Catalytic Processes for Fine and Specialty Chemicals, Elsevier, India, 2016, pp. 187–219.
- [68] F. Zhou, N. Lu, B. Fan, H. Wang, R. Li, Zirconium-containing UiO-66 as an efficient and reusable catalyst for transesterification of triglyceride with methanol, J. Energy Chem. 25 (2016) 874–879.
- [69] F.G. Cirujano, A. Corma, F.X. Llabrés I Xamena, Zirconium-containing metal organic frameworks as solid acid catalysts for the esterification of free fatty acids: synthesis of biodiesel and other compounds of interest, Catal. Today 257 (2015) 213–220.
- [70] Y. Wang, Z. Yang, X. Wu, W. Quan, Q. Chen, A. Wang, UiO-66 with both brønsted and lewis acid sites for catalytic synthesis of biodiesel, Molecules 29 (2024) 4195.
- [71] S.P. Gouda, D. Shi, S. Basumatary, H. Li, R. Piloto-Rodríguez, S.L. Rokhum, Sulfamic acid modified UiO-66 metal-organic framework for biodiesel production: process optimization using response surface methodology, kinetics, and thermodynamic study, Chem. Eng. J. 480 (2024) 148154.
- [72] Y. Li, S. Zhang, Z. Li, H. Zhang, H. Li, S. Yang, Green synthesis of heterogeneous polymeric bio-based acid decorated with hydrophobic regulator for efficient catalytic production of biodiesel at low temperatures, Fuel 329 (2022) 125467.
- [73] H. Li, Z. Han, F. Liu, G. Li, M. Guo, P. Cui, S. Zhou, M. Yu, Esterification catalyzed by an efficient solid acid synthesized from PTSA and UiO-66(Zr) for biodiesel production, Faraday Discuss 231 (2021) 342–355.
- [74] G. Zoppi, E. Tito, I. Bianco, G. Pipitone, R. Pirone, S. Bensaid, Life cycle assessment of the biofuel production from lignocellulosic biomass in a hydrothermal liquefaction–aqueous phase reforming integrated biorefinery, Renew. Energy 206 (2023) 375–385.
- [75] M.H. Rocha, R.S. Capaz, E.E.S. Lora, L.A.H. Nogueira, M.M.V. Leme, M.L.G. Renó, O.A. Del Olmo, Life cycle assessment (LCA) for biofuels in Brazilian conditions: a meta-analysis, Renew. Sustain. Energy Rev. 37 (2014) 435–459.
- [76] H. Kamahara, U. Hasanudin, A. Widiyanto, R. Tachibana, Y. Atsuta, N. Goto, H. Daimon, K. Fujie, Improvement potential for net energy balance of biodiesel derived from palm oil: a case study from Indonesian practice, Biomass Bioenergy 34 (2010) 1818–1824.
- [77] S. Papong, T. Chom-In, S. Noksa-nga, P. Malakul, Life cycle energy efficiency and potentials of biodiesel production from palm oil in Thailand, Energy Pol. 38 (2010) 226–233
- [78] S.P. de Souza, S. Pacca, M.T. de Ávila, J.L.B. Borges, Greenhouse gas emissions and energy balance of palm oil biofuel, Renew. Energy 35 (2010) 2552–2561.
- [79] S. Pleanjai, S.H. Gheewala, Full chain energy analysis of biodiesel production from palm oil in Thailand, Appl. Energy 86 (2009) S209–S214.
- [80] T. Silalertruksa, S.H. Gheewala, Environmental sustainability assessment of palm biodiesel production in Thailand, Energy 43 (2012) 306–314.
- [81] G. Saranya, T.V. Ramachandra, Life cycle assessment of biodiesel from estuarine microalgae, Energy Convers. Manag. X 8 (2020) 100065.

- [82] S. Foteinis, E. Chatzisymeon, A. Litinas, T. Tsoutsos, Used cooking-oil biodiesel: life cycle assessment and comparison with first- and third generation biofuel, Renew. Energy 153 (2020) 588–600.
- [83] M. Branco-Vieira, D.M.B. Costa, T.M. Mata, A.A. Martins, M.A.V. Freitas, N.S. Caetano, Environmental assessment of industrial production of microalgal biodiesel in central-south Chile, J. Clean. Prod. 266 (2020) 121756.
- [84] K. Soratana, W.J. Barr, A.E. Landis, Effects of co-products on the life-cycle impacts of microalgal biodiesel, Bioresour. Technol. 159 (2014) 157–166.
- [85] H.A.R. Mantari M, H.M. Hassim, R.A. Rahman, A.F.M. Zin, M.S. Yahya, N.A. Samiran, N. Asmuin, Techno-economic feasibility of palm fatty acid distillate (PFAD) blend as alternative to diesel fuel, IOP Conf. Ser. Mater. Sci. Eng. 788 (2020) 012064.
- [86] S.Q. Lopes, F.H. Holanda, D.E.Q. Jimenez, L.A.S. do Nascimento, A.N. Oliveira, I.M. Ferreira, Use of Oxone® as a potential catalyst in biodiesel production from palm fatty acid distillate (PFAD), Catal. Lett. 152 (2022) 1009–1019.